Bulletin of Mathematical Biology (2006) 68: 1231–1255
DOI 10.1007/s11538-006-9069-9

ORIGINAL ARTICLE

Transbilayer Pores Induced by Thickness Fluctuations

Liviu Movileanu[a,b,*], Dumitru Popescu[c,d], Stelian Ion[d], Aurel I. Popescu[e]

[a] *Department of Physics, Syracuse University, 201 Physics Building, Syracuse, NY 13244-1130, USA*
[b] *Structural Biology, Biochemistry and Biophysics Program, Syracuse University, Syracuse, NY 13244-4100, USA*
[c] *Faculty of Biology, Laboratory of Biophysics, University of Bucharest, Splaiul Independentei 91–95, Bucharest R–76201, Romania*
[d] *Institute of Applied Mathematics, Calea 13 Septembrie 13, P.O. Box 1–24, Bucharest, Romania*
[e] *Faculty of Physics, Department of Electricity and Biophysics, University of Bucharest, P.O. Box MG 11, Bucharest-Magurele, R–077125, Romania*

Received: 5 October 2004 / Accepted: 18 November 2005 / Published online: 22 April 2006

Abstract Thermally-induced fluctuations of individual phospholipids in a bilayer lipid membrane (BLM) are converted into collective motions due to the intermolecular interactions. Here, we demonstrate that transbilayer stochastic pores can be generated via collective thermal movements (CTM). Using the elastic theory of continuous media applied to smectic-A liquid crystals, we estimate the pore radius and the energetic requirements for pore appearance. Three types of thermally-induced transbilayer pores could be formed through BLMs: open and stable, open and unstable, and closed. In most of the situations, two open and stable pores with different radii could be generated. Notably, the two pores have the same generation probability. Unstable pores are possible to appear across thin bilayers that contain phospholipids with a large polar headgroup. Closed pores are present throughout the cases that we have inspected. The effects of hydrophobic thickness, polar headgroup size of phospholipids, temperature, surface tension, and elastic compression on the pore formation and pore stability have been examined as well.

Keywords Stochastic pores · Bilayer lipid membrane · Oscillations · Deformation free energy · Thickness fluctuations · Pore size

*Corresponding author.
E-mail address: lmovilea@physics.syr.edu (Liviu Movileanu).

Abbreviations a_0, Cross-sectional area per phospholipid; $\overline{B}$, Elastic coefficient of BLM compression; $\overline{B}_s$, Elastic coefficient of solvent layer compression; $\overline{B}_c$, Elastic coefficient of hydrophobic layer compression; BLM, Bilayer lipid membrane; CTM, Collective thermal motion of phospholipids; CR, Compatibility range for the pore formation; ΔE_L, Energy variation due to pore linear contour change; ΔE_S, Energy variation due to pore surface change; ΔF, Deformation free energy change per unit area of lipid bilayer; ΔF_c, Critical free energy barrier corresponding to critical pore radius; γ, Surface tension coefficient; h, Half-thickness of hydrophobic domain; h_l, Half-thickness of hydrophobic domain in the case of BLM with solvent; h_s, Half-thickness of solvent between the two monolayers; h_p, Half-thickness of polar headgroup domain; k_B, Boltzmann's constant; K_c, Curvature elastic modulus; K_l, Elastic coefficient of splay distortion; λ, Deformation wavelength of the lipid bilayer; λ_0, Deformation wavelength λ that corresponds to R_{min} (see below, R_{min}); l, The length of the arc around Oz axis; $\mathbf{n}$, Unit vector (with variable direction) of the deformation wave; N, Number of atoms in a phospholipid; N_b, Number of covalent bonds in a phospholipid; N_c, Number of intra-molecular constraints; N_m, Number of phospholipids involved in collective thermal motion; r_c, Critical radius of a transbilayer pore (maximum radius of a stable pore); r_p, Radius of the pore; R_{min} (R_{max}), Lowest (highest) value of the radius of the perturbed region able to generate stochastic transbilayer pores; r_0, Radius of the pore that corresponds to a perturbed region of radius R_{min} (the radius of the most probable pore); r, Radial variable of the deformation wave function, for the case of cylindrical symmetry; R, Radius of the BLM perturbed region; σ, Line tension; T, Absolute temperature; $u\,(x, y, z)$ Position-dependent displacement from initial unperturbed half-thickness of the membrane; u_s, Deformation of solvent layer.

1. Introduction

Phospholipids, as a major component of biological membranes, undergo three categories of random thermal movements: (i) they can diffuse freely in the bilayer plane, thus conferring a fluid phase state to the membrane; (ii) they can also exhibit self-oscillations and rotations around their longitudinal axes; (iii) they have the ability to randomly fluctuate in a direction that is normally oriented, relative to the lipid bilayer. Because of these features, the bilayer lipid membrane (BLM) is a remarkable self-assembled and flexible structure that can experience a variety of conformational and dynamic transitions (Popescu and Rucareanu, 1992; Sackmann, 1995; Shillcock and Seifert, 1998; Boal, 2001; Holthuis et al., 2003). Furthermore, the artificial and natural BLMs are not perfect insulating systems, but are permeable for water and electrolytes that diffuse across by a diversity of transmembrane pores.

A stochastic transbilayer pore can form and grow, following an activated process brought about by an external trigger. Examples include a short duration and high amplitude electrical pulse (Winterhalter and Helfrich, 1987; Freeman et al., 1994; Saulis, 1997; Bordi et al., 1999; Bordi et al., 2000; Neu et al., 2003; Neu and Krassowska, 2003; Tieleman et al., 2003; Tieleman, 2004), random and biased thermal fluctuations of bilayer thickness (Popescu et al., 1991; Shillcock and

Seifert, 1998; Marrink et al., 2001; Farago, 2003; Fournier and Joos, 2003; Loison et al., 2004; Movileanu and Popescu, 2004; Farago and Santangelo, 2005), and other drastic changes of the cellular environment (Shillcock and Boal, 1996; Moroz and Nelson, 1997; Sung and Park, 1997; Sung and Park, 1998; Karatekin et al., 2003; Leontiadou et al., 2004). The radius of the pores can vary over a wide range, from nanometers to micrometers. Their lifetime is strongly dependent on both the external trigger and intrinsic properties of the membrane. For example, the electroporated pores in membranes can last several microseconds, but the thermally-induced unstable pores show a much shorter lifetime of the order of a few nanoseconds (Marrink et al., 2001; Leontiadou et al., 2004). In an extreme situation, using micropipette extrusion on vesicles, Needham and Zhelev have been able to show the presence of large transbilayer pores with a duration of several seconds (Zhelev and Needham, 1993).

Most of the models for pore formation in membranes are based on a simple hypothesis proposed three decades ago by Litster (Litster, 1975; Sung and Park, 1997; Sung and Park, 1998). A stochastic pore may tend to open or close, depending on the forces acting on its boundary. The appearance of a circular pore of radius r_p in a membrane with surface tension coefficient γ is determined by the presence of two competing energetic terms: a reduction in free energy by a surface tension component ($-\pi r^2\gamma$), and an increase in free energy by a line tension component ($+2\pi r\sigma$). The line tension σ is caused by the hydrophobic property of phospholipids, and contributes to the energy barrier height against pore formation. The surface tension coefficient γ reduces the barrier height for pore formation. Weaver and colleagues (Freeman et al., 1994) have used such a model for electroporation experiments. The model accurately predicts that pores with a size beyond a critical value ($r_p > r_c$) evolve into an unstable structure and may lead to the BLM rupture (Popescu and Margineanu, 1981; Shillcock and Boal, 1996; Fournier and Joos, 2003), whereas smaller pores ($r_p < r_c$) undergo a resealing process (Saulis, 1997; Farago, 2003; Popescu et al., 2003; Farago and Santangelo, 2005). The model that we propose in this paper is, to some extent, similar to the aforementioned approaches. However, the mechanistic details for pore formation differ from the previous models, and are thoroughly presented in the next sections of this article.

Particularly, the presence of BLM hydrophobic thickness fluctuations was demonstrated both by theory (Hladky and Gruen, 1982: Hladky and Gruen, 1984) and experiment (Benz et al., 1975). For a mixture of lipids in BLMs, a selective association between phospholipids takes place, thus generating phospholipid domains and local changes in hydrophobic thickness (Popescu, 1993; Popescu et al., 1997). The phospholipid domain thickness is dependent on the length of the hydrocarbon chain of phospholipids (Popescu and Victor, 1990; Movileanu and Popescu, 1995; Movileanu and Popescu, 1996; Movileanu et al., 1997; Movileanu et al., 1998; Movileanu and Popescu, 1998). The appearance of stochastic pores in BLMs, due to thickness fluctuations, was first proposed by Popescu and colleagues (Popescu et al., 1991).

The height of the energy barrier for membrane perforation due to this mechanism is large ($\sim 91\, k_B T$) (Popescu et al., 1991), where k_B and T are the Boltzmann constant and absolute temperature, respectively. In this case, the geometrical

profile of the pore, on a perpendicular plane to the BLM, is an elliptical toroidal form. It was also shown that such a transmembrane pore could evolve into a stable state. The results obtained by this model were pretty surprising, because of the short time scale for resealing of stochastic pores in membranes. Two years later, Zhelev and Needham (Zhelev and Needham, 1993) created large and quasi-stable pores in lipid bilayer vesicles, in accord with the previous model prediction (Popescu et al., 1991). The membrane resistance to rupture (Popescu and Margineanu, 1981; Shillcock and Boal, 1996), expressed in terms of a line tension for a large pore in bilayer vesicles, has been calculated by Moroz and Nelson (Moroz and Nelson, 1997). Notably, they have suggested a new procedure for an accurate estimate of the line tension using data from Zhelev and Needham's experiment.

In this work, we propose a model for the appearance of either transient or stable transbilayer pores of nanoscopic dimensions, via thermally-induced thickness fluctuations of the lipid membrane. For this purpose, we have used the elasticity theory of continuous media (Huang, 1986; Helfrich and Jakobsson, 1990; Nielsen et al., 1998; Nielsen and Andersen, 2000; May, 2000; Popescu et al., 2003) to describe the appearance of stochastic pores in a lipid membrane. A planar membrane conformation that is stable at zero temperature can become unstable at nonzero temperatures for certain intrinsic elastic membrane parameters and environmental stress conditions. We examine the stability of the membrane and determine the conditions for transbilayer pore formation brought about by fluctuations of the temperature-induced membrane thickness.

The appearance of stochastic transbilayer pores in lipid membranes due to thermal fluctuations has been recently examined by several groups (Popescu et al., 2003; Loison et al., 2004; Farago and Santangelo, 2005). Overall, we show that these transbilayer thickness fluctuations promote the opening, or, in other situations, the closure of the already formed pores. Moreover, we establish the conditions for which the membrane thickness fluctuations stabilize pores of a certain size. The pore radius was estimated on a continuum model, assuming that the BLM deformation free energy is equal to the total thermal energy of the phospholipids that co-participate in the collective thermal motion (CTM).

2. Computing strategy

2.1. BLMs regarded as smectic liquid crystals

We briefly review the BLM physical properties that are relevant for the present work: (i) the phospholipids are oriented along a favored direction, almost perpendicular or slightly tilted, relative to the BLM surface (Helfrich and Jakobsson, 1990; May, 2000; Kessel et al., 2001); (ii) the two monolayers have closely similar thickness and can glide one along the other; (iii) there is no exchange of phospholipids between the two monolayers. The translocation events from one monolayer to the other (e.g., flip–flop transitions) are very improbable (Popescu and Victor, 1991b); (iv) there is a short-range order in each monolayer that is characteristic of liquid crystals. This is because both the dipolar interactions between the

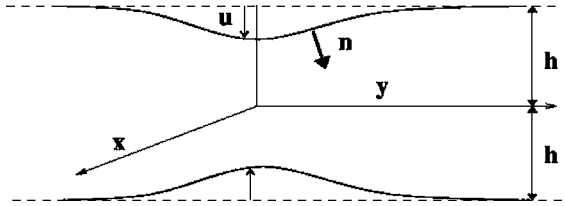

Fig. 1 The local deformation, *u,* of a lipid bilayer produced by collective thermal motion. **n(r)**: the unitary vector, of molecules orientation. *h* is the lipid monolayer thickness.

neutral polar headgroups and the van der Waals-London interactions between the hydrophobic chains are short-range in nature. All these properties are specific to a smectic liquid crystal of A type (De Gennes, 1974; Huang, 1986).

2.2. Deformation free energy

For the reasons mentioned above, it is appropriate to describe the BLM mechanics by the continuous theory of a smectic liquid crystal of A type (Helfrich, 1973; Huang, 1986; Helfrich and Jakobsson, 1990; Popescu et al., 2003). Hereafter, we consider only a homogenous and solvent-free BLM, unless otherwise stated. In nematic liquid crystals, there are four types of deformations: a compression-expansion component, a splay-, a twist-, and a bend-distortion component. The last two are unfavorable in smectic liquid crystals (Huang, 1986). Therefore, the free energy change is dominated by compression-expansion and splay deformation. We assume that the upper BLM boundary undergoes a deformation displacement given by $u(x, y, z) = u(\boldsymbol{r})$ which is evaluated relative to the initial unperturbed position (Fig. 1).

In the case of a small deformation of the BLM accompanied by a large deformation wavelength, the change in deformation free energy per unit volume, according to smectic liquid crystal theory, is given by the following formula (De Gennes, 1974):

$$\Delta F(x, y, z) = \frac{1}{2}\overline{B}\left(\frac{\partial u}{\partial z}\right)^2 + \frac{1}{2}K_1(\operatorname{div}\mathbf{n})^2 \tag{1}$$

where $\overline{B}$ and K_l are the elastic coefficients of membrane compression and splay-distortion, respectively. **n** is the unit vector of the deformation wave.

Because the lateral compression can be expressed as the first order Oz-axis derivative, $\overline{B}$ can be calculated in such a way that the first term of Eq. (1) includes both the transverse and longitudinal compressions. If we integrate Eq. (1) over the BLM thickness (i.e., from 0 to $2h$) and apply the boundary conditions and the condition for minimum deformation free energy, then the expression for ΔF is given by (Huang, 1986; Helfrich and Jakobsson, 1990; Popescu et al., 2003):

$$\Delta F(x, y) = h\overline{B}\left(\frac{u}{h}\right)^2 + hK_1\left(\frac{\partial^2 u}{\partial x^2} + \frac{\partial^2 u}{\partial y^2}\right)^2 \tag{2}$$

where h is the half-thickness of the hydrophobic domain of the lipid bilayer.

Taking into account the energy contribution due to the change in the surface area of the BLM, one can obtain a complete expression for the BLM deformation free energy per unit area (Huang, 1986; Helfrich and Jakobsson, 1990; Popescu et al., 2003):

$$\Delta F(x, y) = \overline{B}\frac{u^2}{h} + hK_1\left(\frac{\partial^2 u}{\partial x^2} + \frac{\partial^2 u}{\partial y^2}\right)^2 + \gamma\left[\left(\frac{\partial u}{\partial x}\right)^2 + \left(\frac{\partial u}{\partial y}\right)^2\right] \tag{3}$$

where γ is the bilayer surface tension coefficient.

The elasticity theory, applied to the BLM, regarded as a continuous media, has the advantage that it takes into consideration the intrinsic properties of the membrane, characterized by the constants $\overline{B}$, K_l, and γ. This was the primary motivation for using elasticity theory to calculate the BLM free energy induced by a surface perturbation.

2.3. BLM thickness fluctuations and pore appearance

There are the following interactions between phospholipids: (i) repulsion/ attraction between the charged headgroups; (ii) attraction between neutral headgroups and (iii) attraction between the hydrophobic chains themselves. Because these interactions are weak and the membrane fulfils the properties of a smectic liquid crystal, the individual motions of the phospholipids in the normal direction on the BLM surface, following a resonance proccess, may be transformed into a collective thermal motion (CTM). This phenomenon can trigger local random changes in the BLM thickness fluctuations. Hladky and Gruen (Hladky and Gruen, 1982) have demonstrated that thickness fluctuations with intermediate deformation wavelength of about 100 Å have a significant probability of occurrence. Here, we show that CTM promotes stochastic BLM perforations (i.e., spontaneous thermoporations). The real deformation of a BLM may be decomposed into simple sinusoidal deformations. Therefore, we consider a local BLM deformation described by a cosine function $u(\mathbf{r})$, with a deformation wavelength λ and with its amplitude h equal to the half-thickness of the hydrophobic domain:

$$u(r) = -h\cos\frac{2\pi r}{\lambda} = -h\cos(kr) \tag{4}$$

where $k = 2\pi r/\lambda$ represents the wave number.

The initial state of the BLM was considered to be that in which molecules do not move at all (i.e., the initial temperature is 0 K). At this temperature, both surfaces of the BLM are planar. By warming the BLM up, the phospholipids obtain kinetic energy and their thermal motions will contribute to the BLM deformations. These deformations are sometimes called "membrane undulations" or "membrane ripples." This phenomenon favours the occurrence of BLM thickness fluctuations. Thus, the collective thermal energy must be equal to or greater than the bilayer deformation free energy. Taking into account that the BLM deformation maintains a cylindrical symmetry, the above condition, for a perturbed patch of radius

R, can be rewritten in polar coordinates (Popescu et al., 2003):

$$\int_0^{2\pi} \mathrm{d}\theta \int_0^R r \left[\overline{B} \frac{u^2}{h} + \gamma \left(\frac{\partial u}{\partial r} \right)^2 + hK_1 \left(\frac{\partial u}{r\partial r} + \frac{\partial^2 u}{\partial r^2} \right)^2 \right] \mathrm{d}r$$

$$= N_{\mathrm{m}} \varepsilon_{\mathrm{c}} = \frac{\pi R^2}{a_0} (3N - N_{\mathrm{c}}) \frac{k_{\mathrm{B}} T}{2}. \tag{5}$$

Here, N_{m} is the number of phospholipids involved in collective thermal motion, N is the number of atoms of a phospholipid, N_{c} is the number of intra-molecular constraints, ε_{c} is the mean kinetic energy of a phospholipid, $\frac{k_{\mathrm{B}} T}{2}$ is the mean kinetic energy associated to a single molecular freedom degree, h is the half-thickness of the lipid bilayer and a_0 is the cross-sectional area of the polar headgroup of phospholipids. For a polyatomic molecule, we have $3N - N_{\mathrm{c}} = 6$.

After integration over θ and multiplication of both terms of Eq. (5) by $\frac{2}{\pi \overline{B} h R^2}$, one obtains:

$$\frac{4}{R^2} \int_0^R r \left[\frac{u^2}{h^2} + \frac{\gamma}{\overline{B} h} \left(\frac{\partial u}{\partial r} \right)^2 + \frac{K_1}{\overline{B}} \left(\frac{\partial u}{r\partial r} + \frac{\partial^2 u}{\partial r^2} \right)^2 \right] \mathrm{d}r - \frac{k_{\mathrm{B}} T}{\overline{B} a_0 h} (3N - N_{\mathrm{c}}) = 0. \tag{6}$$

Taking into account the expression for local BLM deformation, Eq. (4), the derivatives from Eq. (6) are the following:

$$\frac{\partial u}{\partial r} = kh \sin(kr); \quad \frac{\partial^2 u}{\partial r^2} = k^2 h \cos(kr). \tag{7}$$

Using (4) and (7), the left side of Eq. (6) can be split into three terms defined by

$$T_0 = \frac{4}{R^2} \int_0^R r \cos^2(kr) - \frac{k_{\mathrm{B}} T}{\overline{B} a_0 h} (3N - N_{\mathrm{c}}) \tag{8}$$

$$T_1 = \frac{4\gamma}{h \overline{B} R^2} \int_0^R (kh)^2 r \sin^2(kr) \, \mathrm{d}r \tag{9}$$

$$T_2 = \frac{4K_1}{R^2 \overline{B}} \int_0^R r \left[\frac{kh}{r} \sin(kr) + k^2 h \cos(kr) \right]^2 \mathrm{d}r$$

$$= \frac{4K_1}{R^2 \overline{B}} \int_0^R \left[\frac{k^2 h^2}{r} \sin^2(kr) + k^3 h^2 \sin(2kr) + k^4 h^2 r \cos^2(kr) \right] \mathrm{d}r. \tag{10}$$

Introducing the nondimensional parameters: $\alpha = kR$ and $\beta = kh$, one obtains the following expressions for the aforementioned terms (Appendix A):

$$T_0 = 1 + \frac{\sin 2\alpha}{\alpha} - \frac{1 - \cos 2\alpha}{2\alpha^2} - \frac{k_B T}{\overline{B} a_0 h}(3N - N_c) = c(\alpha) \tag{11}$$

$$T_1 = \frac{\gamma}{\overline{B}h}\left(1 - \frac{\sin 2\alpha}{\alpha} + \frac{1 - \cos 2\alpha}{2\alpha^2}\right)\beta^2 = b(\alpha)\beta^2 \tag{12}$$

$$T_2 = \frac{K_1}{\overline{B}h^2}\left(1 + \frac{\sin 2\alpha}{\alpha} + 3\frac{1 - \cos 2\alpha}{2\alpha^2} + \frac{4}{\alpha^2}\int_0^1 \frac{\sin^2(\alpha s)}{s}\mathrm{d}s\right)\beta^4$$

$$= a(\alpha)\beta^4. \tag{13}$$

Taking into account the notations (11)–(13), Eq. (6) can be rewritten

$$a(\alpha)\beta^4 + b(\alpha)\beta^2 + c(\alpha) = 0. \tag{14}$$

Certainly, Eq. (14) is a very complex relation, yielding an implicit formula for λ and R. However, one can use it to obtain their parametrical representations.

Equation (14) is an algebraic relation for β as a function of the parameter α. Since the functions $a(\alpha)$ and $b(\alpha)$ are always positive, Eq. (14) has real solutions only if the function $c(\alpha)$ is negative. If these conditions are simultaneously fulfilled, we get a single positive solution:

$$\lambda(\alpha) = 2\pi h\left(\sqrt{\frac{2a(\alpha)}{-b(\alpha) + \sqrt{b^2(\alpha) - 4a(\alpha)c(\alpha)}}}\right)$$
$$R(\alpha) = \frac{y\lambda(\alpha)}{2\pi}. \tag{15}$$

All the results were obtained by the assumption that the deformation free energy is equal to the total thermal energy of the molecules from the patch of a radius R that co-participate in the CTM. More precisely, the results were obtained by solving Eq. (14) in each particular case.

2.4. Choice of BLM parameters

In this section, we show the conditions under which the thermally-induced thickness fluctuations of the BLM hydrophobic core can generate transbilayer pores. The compressibility coefficient $\overline{B}$, obtained by Hladky and Gruen (Hladky and Gruen, 1982) from the experimental data of White (White, 1978), is equal to $5.4 \times 10^7\,\mathrm{Nm}^{-2}$. The BLM surface area occupied by a single phospholipid is $39\,\text{Å}^2$ (Popescu and Victor, 1991a), while the surface tension coefficient γ is $8 \times 10^{-4}\,\mathrm{Nm}^{-1}$ (Neher and Eibl, 1977; Nielsen et al., 1998). The splay coefficient K_1 was obtained from the experimental data by using the curvature elastic modulus $K_c = (2.8\text{–}6.5) \times 10^{-20}\,\mathrm{J}$ (Engelhardt et al., 1985), in the case of lecithin vesicles. Thus, from $K_1 = K_c/2h$ (Schneider et al., 1984), one can easily obtain the splay coefficient, implemented in Eq. (14). Because the vesicle thickness used for

the experimental measurement of K_c was 30 Å, then K_1 is in the range from 9 to 22×10^{-12} N.

The BLM, as characterized by the parameters $2h = 31$ Å, $a_0 = 39$ Å^2, $K_1 = 9 \times 10^{-12}$ N, $\overline{B} = 5.4 \times 10^7$ Nm^{-2}, $\gamma = 15 \times 10^{-4}$ Nm^{-1} and $T = 300$ K, will be considered as the reference BLM. The curve that corresponds to the reference BLM was marked with "0."

3. Results and discussion

3.1. Types of pores and their stability

3.1.1. Types of pores

In order to generate transbilayer pores, the CTM must employ the phospholipids from a BLM patch with a radius R in the range $[R_{\min}, R_{\max}]$. We simply call this domain a compatibility range (CR) for the pore formation. We show a generalized scheme (Fig. 2) for the dependence of the pore radius r_p (Fig. 2A), and BLM deformation wavelength λ (Fig. 2B), on the CTM radius R. Very interestingly, in most of the cases examined in this work, the BLM deformation wavelength λ is not a *one-to-one function* for all values of R of the perturbed patch of the CR. In other words, there is a sub-domain of R, such that for each value of R, Eq. (14) gives two values for λ (Fig. 2). If we consider λ_0 to be the wavelength value corresponding to $R_{\min}$, then the point $(R_{\min}, \lambda_0)$ on the graph of λ versus R is the nearest point to the λ axis. This point divides each curve $\lambda = \lambda(R)$ into two parts: an upper and a lower branch. Taking into account that the pore radius is a monotonically increasing function of the BLM deformation wavelength, it follows that a pore can be generated for each λ value.

The BLM surface perturbation with a radius $R_{\min}$ is induced by the CTM with the lowest number of phospholipids. The deformation free energy reaches a minimum at $R = R_{\min}$, and the pore generated by this perturbation is the most probable pore, with radius denoted as r_0. The pores generated by the BLM deformation wavelength with $\lambda > \lambda_0$ will have radii $r_p > r_0$, whereas the pores generated by the deformations with $\lambda < \lambda_0$ will have $r_p < r_0$.

First, let us consider R for which the function $\lambda = \lambda(R)$ is not a *one-to-one function*. In Fig. 2, R values are in the range $(R_{\min}, R_{c2}]$. As each value of R can generate two BLM deformations with different wavelengths, then two transbilayer pores with different radii may be created.

Second, let us now consider R for which the function $\lambda = \lambda(R)$ is a *one-to-one function*. This occurs when the values of R pertain to the range $(R_{c2}, R_{\max}]$. In this case, each R corresponds to a single λ, and a single pore could be generated (Fig. 2).

3.1.2. Pore stability

A legitimate question which arises is whether such a stochastic pore is stable or unstable. Generally, the stability criterion is given by the Litster model. According to Litster's model (Litster, 1975), the deformation free energy of a pore with radius r_p, is equal to $\Delta F = 2\pi r_p(\sigma - r_p\gamma/2)$, and the critical free energy barrier for which the radius of the pore attains a critical value $r_c = \frac{\sigma}{\gamma} = \frac{l}{2} \approx h$ (see Appendix B) is

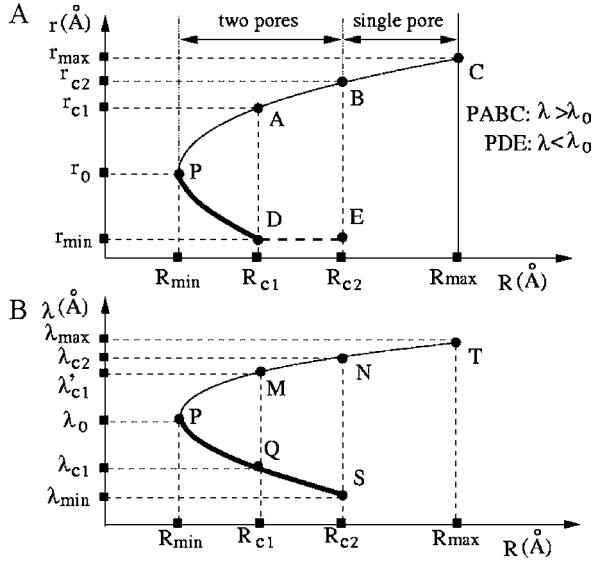

Fig. 2 The dependence on the BLM deformation wavelength, λ, and pore radius, r_p on the perturbation radius R (see comment in the main text).

$\Delta F_c = \pi\gamma\frac{l^2}{4} \approx \pi\gamma h^2$. Therefore, if the pore radius is smaller than the critical value r_c, the force on the pore boundary is inward, the pore radius decreases and the pore reseals. In this case, one says that the membrane is stable. By contrast, if the pore radius is greater than r_c, the pore radius increases indefinitely, thus evolving to BLM rupture (Popescu and Margineanu, 1981; Winterhalter and Helfrich, 1987; Saulis, 1997; Partenskii et al., 1998). In this case, one says that the membrane is unstable. From the point of view of the pore state we can say that in the first case, the pore radius goes towards zero (but the pore may not disappear), and in the second case the pore radius increases indefinitely. In addition, in the first case the pore radius may not decrease to zero. Rather, it may approach a certain stable value, different from zero. In our opinion, in the first case the pore will be stable (open or closed), whereas in the second case the pore is open and unstable. Because the approach presented in this paper does not imply a condition to discriminate between *stable* and *unstable* pores, we use the same formalism for describing the pores generated by surface defects induced by lateral thermal motion.

3.1.3. States of transbilayer pores

The transbilayers pores formed after bilayer perforation may be open ($r_p > 0$) or closed ($r_p \leq 0$). The size of the bilayer patch covered by the CTM may be smaller then λ/4 (Fig. 3a) or greater then λ/4 (Fig. 3b and 3c). By equating the bilayer volume involved in deformation before and after perforation, one obtains the pore radius (Popescu et al., 2003). If the pore radius has a positive value ($r_p > 0$), the pore is in an open state (Figs. 3a, 3b, and 4a). If the solution for pore radius has a negative value ($r_p \leq 0$), the pore is in a closed state (Figs. 3c and 4b). In fact, its radius is equal to zero.

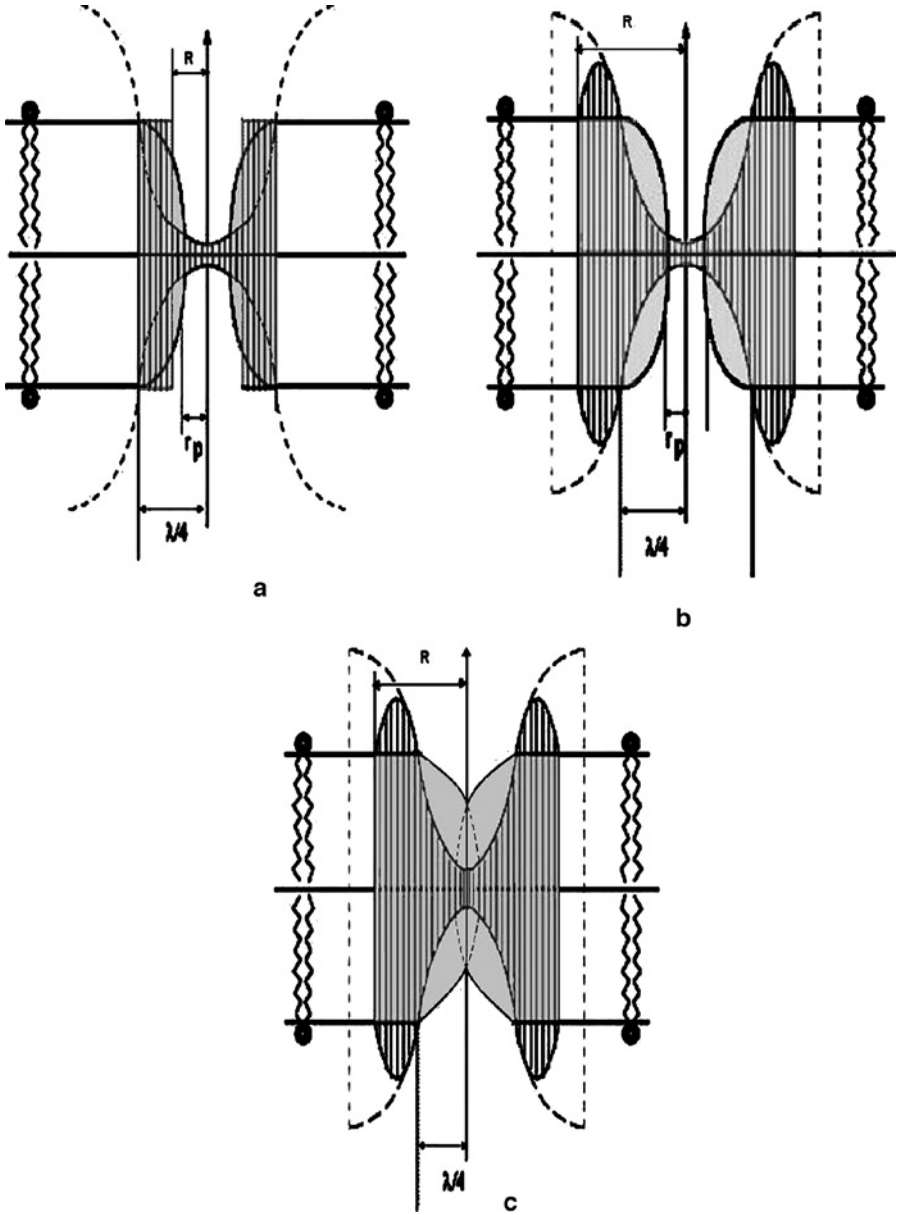

Fig. 3 The perforation of the locally-deformed lipid bilayer due to thickness fluctuations induced by CTM. (a) $R \leq \lambda/4$, only open pores may appear in this case. When $R \geq \lambda/4$, open pores can be generated (b) for nearly all values of λ for which $\lambda/4 \leq R$. Sometimes, for the lowest values of λ, closed pores with a radius $r_p \leq 0$ can be generated (c). These λ values are marked on the bottom end of curves $\lambda = \lambda(R)$ from Figs. 5 and 6. Area marked by vertical lines: the volume occupied by the lipid molecules participating to CTM, just before the BLM perforation. Grey area: the volume occupied by the lipid molecules participating to CTM, after the BLM perforation. The pore radius is inferred from the equality of these two volumes.

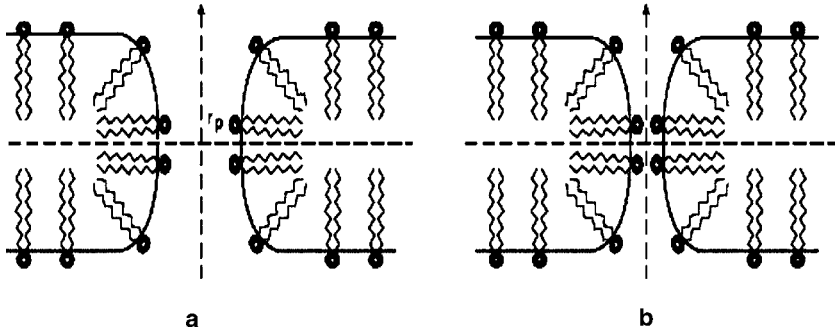

Fig. 4 Two types of transbilayer stochastic pores generated by the BLM thickness fluctuations: (a) open pore; (b) closed pore. The radius of the pore was indicated by r_p. Each phospholipid molecule is represented by its headgroup (a *black circle*) attached to two wiggle hydrophobic tails.

We consider that the pores are stable if their radii, r_p are smaller than the half-thickness of the hydrophobic domain ($r_p < h$). In conclusion, one can say that the CTM can generate three types of transbilayer stochastic pores: *stable* (open or closed/zippered) and *unstable* (open) (Fig. 4). The unstable open pores (i.e., with $r_p > h$) evolve to BLM rupture, because their radii may increase indefinitely.

3.2. Effects of the phospholipid chain length

In this work, we consider three BLMs with values for the hydrophobic thickness $2h$ of 21 Å, 31 Å, and 41 Å, respectively, unless otherwise stated. Taking into account that the half-thickness of the polar headgroup layer, h_p, is about 5 Å, then the BLMs have a full thickness of 31 Å, 41 Å and 51 Å, respectively.

The dependences of the BLM deformation wavelength, λ, and pore radius, r_p, on the size of perturbed region, R, are represented in Fig. 5.

For $2h = 21$ Å, the dependence of the BLM deformation wavelength, λ, on the radius R is a decreasing function, which means that a single pore can be generated. This transbilayer pore may be either open, with its radius lower than 10 Å, or closed (data not shown here).

In contrast with thin bilayers, for $2h = 31$ Å, λ is no longer a *on–to-one function* for the entire CR (Fig. 5, curve 0). For each R (excepting $R = R_{min}$) Eq. (14) gives two solutions for λ. As discussed above, a pore can be generated with either of the two different geometrical states, but with the same deformation free energy. For the case of reference BLM thickness, $R_{min} = 25$ Å corresponds to $\lambda_0 = 88$ Å and $r_0 \approx 12$ Å (Fig. 5B, curve 0). For deformation wavelengths lower than λ_0, the pore radius, r_p, is lower than r_0. For deformation wavelengths greater than λ_0, the pore radius is situated in the range 12–15 Å. For deformation wavelengths belonging to lower branch of curve, corresponding to non one-to-one function, the radii of the pores satisfy the condition: $4\,\text{Å} \leq r_p \leq 12\,\text{Å}$. Both of these states are stable, because r_0 is always smaller than r_c. For λ that corresponds to values located on the lower branch of the graph $\lambda = \lambda(R)$ (Fig. 5A, curve 0), either a single open and stable pore with radius shorter than 4 Å, or a closed pore can be generated (Fig. 5A and 5B, curve 0).

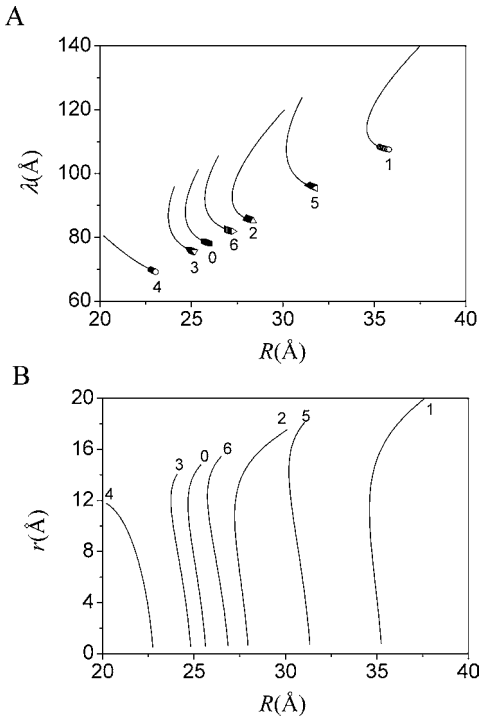

Fig. 5 Dependence of the BLM deformation wavelength λ (A) and of the pore radius, r_p, on the perturbation radius, R (B). Curves marked with zero (0) are describing reference BLM; curves 1, hydrophobic thickness $2h = 40.5$ Å; curves 2, the phospholipid cross-sectional area $a_0 = 45$ Å^2; curves 3, the absolute temperature of 320 K; curves 4, the elastic compression coefficient $\overline{B} = 2.0 \times 10^7$ Nm^{-2}; curves 5, elastic splay coefficient, $K_1 = 22 \times 10^{-12}$ N. The region from each plot situated at the end of the lower branch (indicated by scattered graph) in A corresponds to closed transbilayer pores. The other parameters of the BLM in plots 1–6 are equal to the values of the reference BLM ($2h = 31$ Å, $a_0 = 39$ Å^2, $T = 300$ K, $\overline{B} = 5.4 \times 10^7$ Nm^{-2}, $K_1 = 9 \times 10^{-12}$ N, $\gamma = 15 \times 10^{-4}$ Nm^{-1}).

For a bilayer with $2h = 41$ Å, several types of pores can be generated (Fig. 5A, curve 1). For $\lambda_0 \approx 115$ Å and $R_{\min} \approx 35$ Å, we found that the most probable pore radius is $r_0 \approx 11$ Å. If λ is greater than λ_0 (Fig. 5A, curve 1, upper branch), the pore is stable and $r_p > r_0$ (Fig. 5B, curve 1, upper branch). If λ is smaller than λ_0 (Fig. 5A, curve 1, lower branch), two open and stable pores with two different geometrical stable states may be generated: narrow pores with radii, $r_p < 11$ Å, and closed pores. The model also predicts that if λ is greater than 130 Å, with $\lambda(R)$ located on the upper branch of the graph (Fig. 5A, curve 1), the pores are wide and have only a single state. The transbilayer pores generated by the deformation wavelengths greater than 130 Å will be in a stable state, if their radii are shorter than the critical radius of 20 Å. If their radii are longer than 20 Å, they will evolve to the BLM rupture (Popescu and Margineanu, 1981; Winterhalter and Helfrich, 1987; Saulis, 1997; Partenskii et al., 1998).

3.3. Effects of cross-sectional area of the polar headgroups

The area of the BLM surface occupied by a single molecule depends on the degree of hydration and on the tilting angle made by phospholpid molecule axis with the BLM plane. The polar headgroup size can influence the parameters of Eq. (14), particularly the elastic compressibility, $\overline{B}$, and the surface tension coefficient, γ (see above). We examined a BLM with the thickness of the reference BLM, but with a value for greater cross-sectional area of the polar headgroup of 45 Å^2. In Fig. 5, curve 2, for $a_0 = 45$ Å^2, a new combination of pore states can be generated, compared to the case for which the cross-sectional area value is $a_0 = 39$ Å^2 (the reference BLM). For $R_{\min} < R < 28$ Å, we found that the pore can be either closed or open. In the latter case, the pore radius is smaller than the critical radius of 15 Å. For $R > 28$ Å, the pore can be stable and closed, or it can be unstable, thus triggering the BLM rupture.

The number of phospholipids co-participating in the BLM perturbation decreases with an increase in temperature, because the thermal energy is the unique source of energy attributed to the BLM deformation. Therefore, the probability of transbilayer pore generation increases with the temperature. This conclusion is confirmed by the solutions of Eq. (14) for the reference BLM, for two temperatures, 300 and 320 K, below the phase transition temperature of the BLM (Fig. 5, curves 0 and 3, respectively). The temperature enhancement alters the narrow pore when the conditions are favorable for generation of the two pores. The minimum radius of the narrow pore increases from 4 to 8 Å. Therefore, the increase in temperature affects only the radius of the stable pore that has an open state.

3.4. Effects of the elastic compression and splay

Compressibility properties have a significant effect on the transbilayer pore formation. If Eq. (14) is solved for $\overline{B} = 2 \times 10^7$ Nm^{-2}, then λ is a monotonically decreasing function of R (Fig. 5A, curve 4), which eliminates the possibility of pore appearance with two geometric states. The pores are either open, with a short radius or closed. A change in compression elastic constant from 5×10^7 to 2×10^7 Nm^{-2} determined a shape distortion of the curve $\lambda = \lambda(R)$. There is a critical value ($\overline{B}_c \approx 4 \times 10^7$ Nm^{-2}), beyond which these types of changes occur. For $\overline{B}$ greater than $\overline{B}_c$, the deformation wavelength dependence on the perturbed region radius, R, does not have a *one-to-one* correspondence. From Fig. 5, curve 4, we can infer that only the curve "branch" of the higher values of the wavelength is influenced by the increase in compression elastic constant. For $\overline{B}$ values smaller than $\overline{B}_c$, the dependence of the wavelength λ on the perturbed region radius R becomes a *one-to-one function*, and the range of the wavelength spectrum is narrowed, as $\overline{B}$ decreases.

If the value of the splay elastic constant of the reference BLM ($K_1 = 9 \times 10^{-12}$ N) is replaced by a maximum value of $K_1 = 22 \times 10^{-12}$ N, then R, λ, and r_p are shifted towards higher values (Fig. 5A, curve 5) as compared with the reference BLM. Taking into account that the number of molecules involved in CTM is higher when $K_1 = 22 \times 10^{-12}$ N, then the transbilayer pore appearance is a less

favourable process. The shortest radius of perturbation produced by the CTM is $R_{\min} = 30$ Å, which corresponds to a deformation wavelength of 108 Å.

3.5. Effects of lipid bilayer hydration

In order to examine the hydration effect, we selected two sets of BLMs. The results are plotted in Fig. 6. The first set contains the following: (a) the reference unhydrated BLM ($2h = 31$ Å, $a_0 = 39$ Å^2, curve 0); (b) the hydrated BLM with the same hydrophobic thickness ($2h = 31$ Å, $a_0 = 59$ Å^2, curve 1), designated as hydrated BLM; (c) the hydrated BLM with reduced hydrophobic thickness ($2h = 25$ Å, $a_0 = 59$ Å^2, curve 2), designated as hydrated and thin BLM; (d) the hydrated BLM for which one takes into account the two secondary effects of decrease of hydrophobic thickness and decrease of elastic compression ($2h = 25$ Å, $a_0 = 59$ Å^2 and $B = 5 \times 10^6$ Nm^{-1}, curve 3). The hydrated BLM described in (d) is designated as soft and thin hydrated BLM.

The second set of BLMs contains only two bilayers: (e) an unhydrated thicker BLM ($2h = 41$ Å, $a_0 = 39$ Å^2, marked by "*"), and (f) a partially hydrated BLM ($2h = 34$ Å, $a_0 = 59$ Å^2, curve 4) (Rawicz et al., 2000). We found the following values of the most probable pore radius: (1) for the reference BLM, $r_0 = 12$ Å ($\lambda_0 = 88$ Å, $R_{\min} = 25$ Å), (2) for the hydrated BLM (curve 1), $r_0 = 6$ Å ($\lambda_0 = 128$ Å, $R_{\min} = 41$ Å), (3) for the hydrated and thin BLM (curve 2), $r_0 = 10$ Å ($\lambda_0 = 93$ Å), (4) for the soft and thin hydrated BLM (curve 3), $r_0 = 13$ Å ($\lambda_0 = 85$ Å, $R_{\min} = 22$ Å). Because the number of phospholipids involved in CTM is lower in the hydrated BLM than in the unhydrated one, we conclude that the probability of a stochastic pore is higher in hydrated BLMs. For the modified BLM, due to all secondary effects of hydration (thinner and soft BLM), a single open and stable pore ($r_p \leq 13$ Å) or a closed one can be generated (Fig. 6, curve 3). If the hydrated BLM has a thick hydrophobic domain, then it is more resistant to the thermoporation. This may be seen in Fig. 6, curves "*" and "4," corresponding to the BLM of the second set. Overall, the probability of a stable pore increases with the hydration. This is because the number of lipid molecules necessary for stable pore formation decreases after BLM hydration. It is worth mentioning that the effect of a larger polar headgroup (e.g., hydration of BLM) should be the same as the effect of a lower temperature (Figs. 5 and 6).

3.6. Solvated BLMs

We consider a BLM that contains between its monolayers a non miscible solvent, which is different from water. In this case, there are three layers: two layers are formed by the lipid monolayers with liquid crystal properties and one layer is formed by the solvent situated in between the two monolayers. The solvent thickness is denoted by $2h_s$, and the hydrophobic chain thickness of each lipid monolayer is denoted by h_l. The compression of a BLM due to solvent must be analyzed in two cases:

1. The elastic deformation u is smaller than the half-thickness of the solvent ($u < h_s$). In this case, the BLM compression is mainly given by the solvent

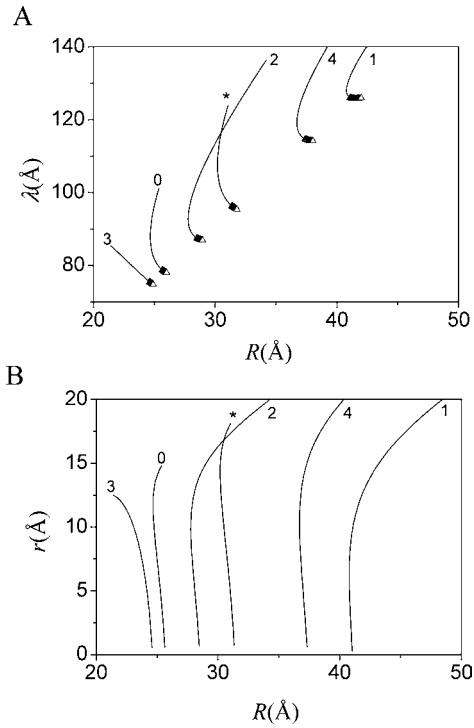

Fig. 6 Dependence of the BLM deformation wavelength λ (A) and of the pore radius, r_p, on the perturbation radius, R (B). Curves marked with zero (0) are describing reference BLM; curves 1, hydrated BLM with a high cross-sectional polar headgroup $a_0 = 59\,\text{Å}^2$, $2h = 31$ Å; curves 2, hydrated BLM with $2h = 25$ Å and $a_0 = 59\,\text{Å}^2$; curves 3, hydrated BLM with $2h = 25.2$ Å, $a_0 = 59\,\text{Å}^2$ and $B = 5 \times 10^6\,\text{Nm}^{-2}$ taking into account the change in the lateral compression; curves marked with (*), thin unhydrated BLM, with $2h = 40.5$ Å and $a_0 = 39\,\text{Å}^2$; curves 4, hydrated BLM with $2h = 34$ Å and $a_0 = 59\,\text{Å}^2$. The region from each plot situated at the end of the lower branch (indicated by scattered graph) from graph (A) corresponds to closed pores. The other parameters of the lipid bilayer in plots 1–4 are equal to the values of the reference BLM (curves 0, see Fig. 5 or the main text).

compression. The resistance to compression between the two media is equivalent to two serial resistances and the equivalent compressibility coefficient, B, is given by the expression (Helfrich and Jakobsson, 1990):

$$B = \frac{B_s B_l}{B_s + B_l}. \tag{16}$$

Because the elastic compressibility coefficient of the solvent is smaller than that for the lipid domain ($\overline{B}_s = 5.4 \times 10^4\,\text{Nm}^{-2}$ and $\overline{B}_l = 5.8 \times 10^7\,\text{Nm}^{-2}$) and because $\overline{B}$ is approximately equal to $\overline{B}_s$, the free energy due to compression is small. The compressed solvent runs laterally within the exterior region of compression (Fig. 7a);

2. The deformation u is greater than the half-thickness of the solvent ($h_s < u < h_l + h_s$). In this case, the solvent compression is followed by the lipid monolayer

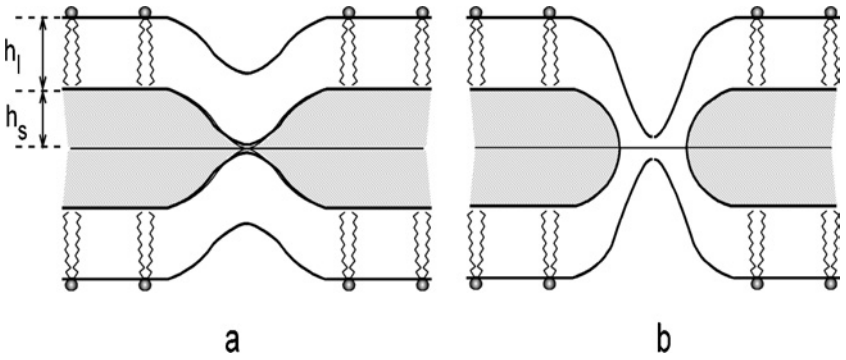

Fig. 7 BLM deformations, u, in the presence of the solvent layer ($2h_s$): (a) the magnitude of lipid bilayer deformation is significantly reduced compared to half-thickness of the solvent layer. Compression is due mainly to the solvent compression; (b) the magnitude of deformation is greater than the half-thickness of the solvent layer. Compression is mainly generated within the hydrophobic domain of the BLM (h_l). Grey is the region occupied by the solvent. Each phospholipid molecule is represented by its headgroup (a *black circle*) attached to two wiggle hydrophobic tails.

compression (Fig. 7b), and will be presented below for transbilayer pore formation (u is equal to $h = h_s + h_l$). The free energy change of the unit area, due to BLM deformation can be calculated according to the following formula (Popescu et al., 2003):

$$\Delta F(x, y) = \overline{B}_s \frac{u_s^2}{h_s} + \overline{B}_l \frac{(u - u_s)^2}{h - h_s} + (h - h_s) K_1 \left(\frac{\partial^2 u}{\partial x^2} + \frac{\partial^2 u}{\partial y^2} \right)^2 + \gamma \left[\left(\frac{\partial u}{\partial x} \right)^2 + \left(\frac{\partial u}{\partial y} \right)^2 \right] \tag{17}$$

where u_s represents the deformation of solvent layer.

The reference BLM has been modified by introducing between the two monolayers a nonmiscible solvent layer with thickness $2h_s = 20$ Å. As we can see in Fig. 8A, curve 1, the wavelength $\lambda = \lambda(R)$ is a monotonically decreasing function. Therefore, a single stable pore can be generated. The pore has a larger radius than that of the solvent-free reference BLM. The higher value of the pore radius results because both the CTM and BLM deformation wavelength λ are greater.

Let us consider a BLM (Fig. 8A, curve 2) with a hydrophobic thickness of 10 Å ($h_l = 10.3$ Å), but with a similar solvent thickness ($h_s = 10$ Å). Then we have a BLM with a full thickness of 41 Å (Fig. 8A, curve 3) which was examined in one of the previous sections (Fig. 5, curve 1). The presence of solvent increase has a very important effect on the pore formation: the number of molecules involved in the CTM is much smaller than it is in the case of the BLM with the same thickness, but without solvent. In addition, the closed pores could not be generated in the presence of solvent. Interestingly, we found that the solvent increases the probability of a stable pore, as well as the probability of the BLM stability. The generation of unstable pores that will evolve to the BLM breakdown is ruled out. Taking

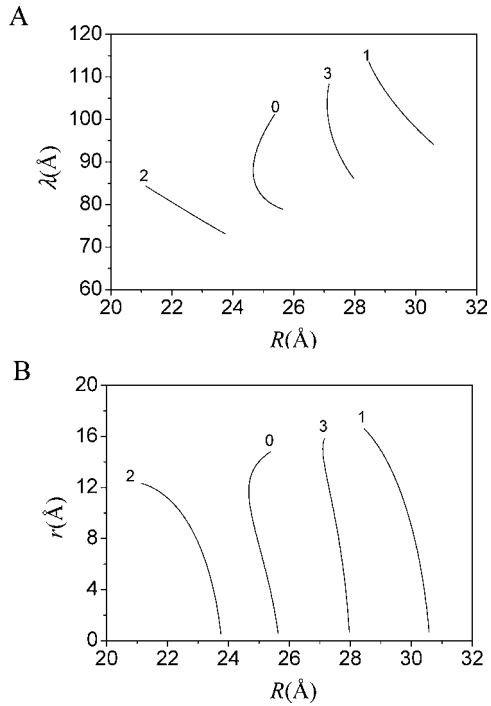

Fig. 8 Dependence of the BLM deformation wavelength, λ (A) and of the pore radius, r_p, on the perturbation radius, R, in the presence of solvent (B). Curves marked with zero (0) are describing the reference BLM, that is, without solvent ($h_s = 0$); curves 1, the reference BLM that includes a solvent layer with the thickness $2h_s = 20$ Å; curves 2, BLM with a total thickness equal to 41 Å, and the solvent thickness represents $2h_s = 20$ Å; curves 3, BLM with the thickness equal to 4.5 Å and with the solvent layer thickness ($2h_s = 20$ Å) and an increased hydrophobic region ($2h_l = 31$ Å).

into consideration that the solvent minimizes the coupling between the monolayers (by minimizing the overlapping between the hydrophobic chains), we conclude that the solvent has a favorable role on the BLM stability.

4. Summary and concluding remarks

There is significant evidence indicating that transient pores of nanoscopic dimensions can stochastically form and evolve in a planar lipid bilayer or a cell membrane, following an activated process induced by an external trigger, such as thermal fluctuations, transmembrane electrical potential, mechanical stress or other changes in the cellular environment. Specifically, the mechanism of pore formation by thermal fluctuations is not clearly understood, but is still a matter of challenge and various controversies (Shillcock and Boal, 1996; Shillcock and Seifert, 1998; Fournier and Joos, 2003; Farago, 2003; Loison et al., 2004; Farago and Santangelo, 2005). Here, we demonstrate that the general theory of continuous elastic media (Helfrich, 1973; Huang, 1986; Helfrich and Jakobsson, 1990;

Partenskii et al., 1998) can predict, for a specific set of intrinsic bilayer parameters, the generation of pores with different sizes and stabilities. The mechanism of the pore formation is caused by thermally-induced thickness fluctuations (Hladky and Gruen, 1982; Hladky and Gruen, 1984), thus involving the CTM of phospholipids perpendicularly oriented on the BLM surface (Popescu et al., 2003; Movileanu and Popescu, 2004). In this work, our major assumption is that the BLM deformation free energy is equal to the total thermal energy of the phospholipids that co-participate in the CTM and produce eventually the transbilayer pore. We did not examine the probability of the pore formation, lifetime of the pore (e.g., "on" and "off" rates), and the pore density. We plan to fully address these issues in a future publication.

Interestingly, this model shows that a bilayer patch of radius R involved in a CTM can produce two bilayer deformations with different wavelengths, one with $\lambda > \lambda_0$, and one with $\lambda < \lambda_0$. These BLM deformations generate individual pores with a radius $r > r_0$, and $r < r_0$, respectively. However, these distinct stochastic pores do not appear simultaneously, and different cases are discussed in this paper.

The theory can be generally applied to other membranes that have a variety of pores. In this case, the elastic coefficient of the BLM compression must be modified, as this depends strongly on the the presence of other pores in bilayer.

Values of the open pore radii, derived in this work, are in agreement with those encountered in the literature, whereas the closed pore formation confirms an old hypothesis concerning the existence of water "threads" into the hydrophobic region of the BLMs (Marrink et al., 2001; Tieleman et al., 2003; Leontiadou et al., 2004;Tieleman, 2004).

Marrink and colleagues (Tieleman et al., 2003) have used molecular dynamics (MD) simulations to detect, at an atomic level, the transient pore formation in a lipid bilayer by mechanical stress and electric fields. Their simulations demonstrated that the pore stability is strongly dependent on the loading rate in MD simulations. The pores are stable at low loading rate, but they are unstable at high loading rate. For high loading rates, an initial pore continue to grow until the bilayer is destabilized. The main reason for which their transient pores are unstable is that the mechanical stress generates a significant BLM thinning at high surface tensions. Marrink and co-workers have observed that the pore stability diagram under mechanical stress can be split in two regimes (Leontiadou et al., 2004). Hydrophilic pores are stabilized for surface tensions lower than a critical threshold of about 38 mN/m. The pores are unstable for surface tensions higher than this value. In a recent paper, Tieleman presents a different molecular mechanism for pore formation under applied electric field (Tieleman, 2004). The probability of pore formation seems to be increased by the presence of local membrane defects involving either water molecules or polar headgroups trapped into the hydrophobic region of the bilayer. For electroporation, the pore formation is determined by the presence of single-file like water defects penetrating into the bilayer and interacting with the local electric fields. Interaction of the water molecules with the local electric fields is an essential step for accelerating the process of pore formation (Tieleman et al., 2003; Tieleman, 2004).

As presented in this work, the transbilayer pores can be generated, if the radius of the CTM is in the range $[R_{\min}, R_{\max}]$. CTM, with a radius shorter than $R_{\min}$ or

longer than R_{max}, produces BLM deformations with magnitudes lower than the half-thickness of the bilayer, so that pore generation is ruled out. In many cases examined in this paper, the pores can exhibit two geometrical states with small or large pore possessing two physical properties: the large pore may be stable or unstable, while the small may only be stable (open or closed, Fig. 2). However, for a thin BLM, only a single type of pore can be generated. The complexity of pore formation increases with the increase in bilayer thickness. The possibility of two different types of pores is also ruled out when the elastic coefficient of BLM compression is low. We found that the BLM stability is increased by the presence of hydration and nonmiscible solvent layers. From a thermodynamic point of view, the two pore states, corresponding to the same R, exhibit similar generation probability. As we mentioned above, the particular values of the deformation wavelength λ indicate which of the two states of the pore will be generated. Taking into account that the thermal energy necessary to induce the BLM deformation is proportional to R^2, we conclude that the closer to R_{min} is the CTM radius, the greater is the probability of a stochastic pore. The model predicts accurately that in bilayers that contain solvent, the probability of stable open pores increases. This aspect of the simulations might explain the behavior of painted bilayers (that contain solvent) as somewhat "leakier" membranes (Hanke and Schlue, 1993).

Undoubtedly, the presence of metastable hydrophilic pores in equilibrium membranes has fundamental importance for both fundamental science and medical biotechnology. Such transbilayer metastable pores can become stable under different environment conditions. The stochastic pores in membranes may represent intermediate states in phase transitions, membrane fusion and budding. The electroporation of cells and lipid vesicles may be used in several biotechnological applications, such as cell transfection, drug delivery and gene therapy. Finally, the formation and stability of the stochastic pores are very complex, because they depend on many intrinsic properties of the lipid bilayers as well as several environmental parameters, including temperature, electric potential, mechanical stress, pH, ionic strength.

Appendix A

Taking into account the following trigonometry relations:

$$\sin^2(kr) = \frac{1-\cos(2kr)}{2} \quad \text{and} \quad \cos^2(kr) = \frac{1+\cos(2kr)}{2}. \tag{A.1}$$

the terms given by the Eqs. (8)–(10) (see the main text) become

$$T_0 = \frac{4}{R^2}\int_0^R r\frac{1+\cos(2kr)}{2}\mathrm{d}r - \frac{k_BT}{\overline{B}a_0h}(3N-N_c) \tag{A.2}$$

$$T_1 = \frac{4\gamma}{h\overline{B}R^2}\int_0^R (kh)^2 r\frac{1-\cos(2kr)}{2}\mathrm{d}r \tag{A.3}$$

$$T_2 = \frac{4K_1}{R^2\overline{B}} \int_0^R \left[\frac{k^2h^2}{r} \sin^2(kr) + k^3h^2 \sin(2kr) + k^4h^2 r \frac{1+\cos(2kr)}{2} \right] \mathrm{d}r. \quad \text{(A.4)}$$

Taking also into consideration the following integrals I_1, I_2, I_3:

$$I_1 = \int_0^R r \cos^2(kr)\,\mathrm{d}r = \frac{R\sin(2kR)}{2k} - \frac{1-\cos(2kR)}{4k^2} \quad \text{(A.5)}$$

$$I_2 = \int_0^R \sin(2kr)\,\mathrm{d}r = \frac{1-\cos(2kR)}{2k} \quad \text{(A.6)}$$

$$I_3 = \int_0^R \frac{\sin^2(kr)}{r}\mathrm{d}r = \int_0^1 \frac{\sin^2(kRs)}{s}\mathrm{d}s \quad \text{(A.7)}$$

entering into the calculation of T_0, T_1, and T_2, one obtains the final expressions of the T_0, T_1, and T_3, as they appear in the Eqs. (11)–(13) (with the notations $\alpha = kR$ and $\beta = kh$).

Appendix B

Let us consider that in the initial state, in a coordinate system with its origin in the middle of the bilayer and the Oz axis oriented perpendicularly on the bilayer surface (Fig. B1), a pore is characterized by

1. its radius as a function of ordinate, z: $r_p(z)$;
2. $r_0 = r(0)$ its neck radius;
3. the line tension, σ, defined as the free energy change due to the modification of the pore neck contour by an unity of length;
4. the surface tension, γ_p, defined as the free energy change due to the modification of the pore by an unity of surface.

This initial state is marked as state "1" and all the parameters referred to it are marked with index "1." Similarly, we mark the state "2" and its parameters.

Now, one increases the pore radius, r_0, from the initial value, $r_1(0)$, to final state, $r_2(0)$. We have noted S_1, S_2 and L_1, L_2 the pore internal surface area, and the pore neck contour, respectively:

$$S_1 = 2\pi \int_{-h}^{+h} r_1(z)\sqrt{1+\left(\frac{\mathrm{d}r_1}{\mathrm{d}z}\right)^2}\,\mathrm{d}z; \quad S_2 = 2\pi \int_{-h}^{+h} r_2(z)\sqrt{1+\left(\frac{\mathrm{d}r_2}{\mathrm{d}z}\right)^2}\,\mathrm{d}z \quad \text{(B.1)}$$

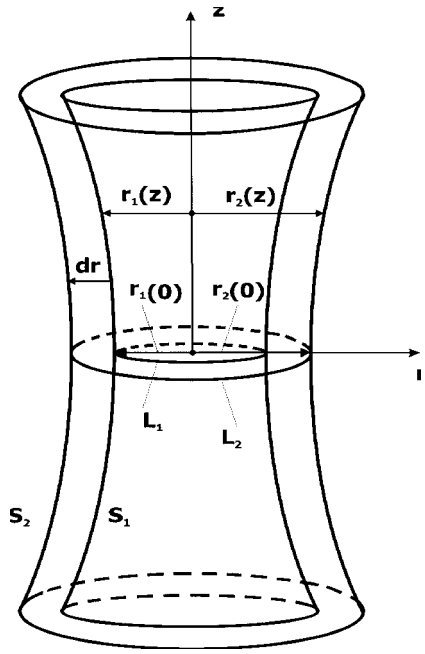

Fig. B1 Two parallel positions of the pore surfaces separated by a distance equal to Δr. $r_1(0)$ and $r_2(0)$ are the neck radii (i.e., $z = 0$) of S_1 and S_2 respectively. The figure is used to demonstrate the relation between the line tension, σ, and the surface tension, γ, that characterize the state of a pore, according to Litster's model (see also the text).

$$L_1 = 2\pi r_1; \quad L_2 = 2\pi r_2. \tag{B.2}$$

Let us assume that the two surfaces are "parallel" one to another (Fig. B1), and $r_2(z) - r_1(z) = \Delta r$. We also assume that $L_2 - L_1 = 2\pi\,\Delta r = 1$ (for a unity length variation).

Therefore, $\frac{\mathrm{d}r_1}{\mathrm{d}z} = \frac{\mathrm{d}r_2}{\mathrm{d}z}$.

The energy change, ΔE_L, due to the increase of linear contour of pore by one length unity is

$$\Delta E_L = \sigma(L_2 - L_1) = \sigma. \tag{B.3}$$

The corresponding energy change, ΔE_S, due to surface change is

$$\Delta E_S = \gamma_p(S_2 - S_1) = 2\pi\,\Delta r\, l\gamma_p = l\gamma_p \tag{B.4}$$

where, γ_p is surface tension of the pore interface, which is nearly equal with surface tension, γ, of a monolayer (i.e., half-bilayer surface tension), and l is the length of the arc whose rotation around Oz axis generate the pore.

Equating ΔE_L, from (B.3) with ΔE_S from (B.4), one obtains that $\sigma = l\gamma_\mathrm{p}$. Measuring electrical tension for lipid bilayer breakdown, the data have been fitted using $\sigma = \overline{h}\gamma_p$, in order to find the coefficient, γ. In this formula, $\overline{h}$ is the entire

hydrophobic thickness of planar lipid bilayer ($\overline{h}$ is two times h used in this work, Pastushenco et al., 1979).

In these conditions, the critical radius, r_c, from the formula of Litster, is equal to $r_c = \frac{l}{2}$. In this work, we approximated $l \approx 2h$ and $r_c = h$. The equality is available for cylindrical pores.

Acknowledgements

We thank anonymous reviewers for their helpful suggestions to the manuscript. Stimulating discussions with Professors Constantin Fetecau and Allen Miller are highly appreciated. LM thanks Prof. Mathias Winterhalter for fruitful discussions during the 2005 Summer School of Biophysics in Bremen. We are also indebted to Alin Gabriel Popescu for his dedicated work on some of the figures. Support of this research by Romanian Ministry of Education and Research (Grant 5003/A10/2002) and Syracuse University start-up funds are gratefully acknowledged.

References

Benz, R., Frohlich, O., Lauger, P., Montal, M., 1975. Electrical capacity of black lipid films and of lipid bilayers made from monolayers. Biochim. Biophys. Acta 394, 323–334.

Boal, D.H., 2001. Mechanics of the Cell. Cambridge University Press, Cambridge.

Bordi, F., Cametti, C., Motta, A., 2000. Ion permeation across model lipid membranes: A kinetic approach. J. Phys. Chem. B 104, 5318–5323.

Bordi, F., Cametti, C., Naglieri, A., 1999. Ion transport in lipid bilayer membranes through aqueous pores. Coll. Surf. A 159, 231–237.

De Gennes, P.-G., 1974. The Physics of Liquid Crystals. Clarendon Press, Oxford.

Engelhardt, H., Duwe, H.P., Sackmann, E., 1985. Bilayer bending elasticity measured by fourier-analysis of thermally excited surface undulations of flaccid vesicles. J. Phys. Lett. 46, L395–L400.

Farago, O., 2003. "Water-free" computer model for fluid bilayer membranes. J. Chem. Phys. 119, 596–605.

Farago, O., Santangelo, C.D., 2005. Pore formation in fluctuating membranes. J. Chem. Phys. 122, 1606–1612.

Fournier, L., Joos, B., 2003. Lattice model for the kinetics of rupture of fluid bilayer membranes. Phys. Rev. E 67, 5190–5197.

Freeman, S.A., Wang, M.A., Weaver, J.C., 1994. Theory of electroporation of planar Bilayer-membranes: Predictions of the aqueous area, change in capacitance, and pore–pore separation. Biophys. J. 67, 42–56.

Hanke, W., Schlue, W.-R., 1993. Planar Lipid Bilayers. Methods and Applications. Academic Press, London, UK.

Helfrich, W., 1973. Elastic properties of lipid Bilayers: Theory and possible experiments. Z. Naturforsch. C28, 693–703.

Helfrich, P., Jakobsson, E., 1990. Calculation of deformation energies and conformations in liquid membranes containing gramicidin channels. Biophys. J. 57, 1075–1084.

Hladky, S.B., Gruen, D.W.R., 1982. Thickness fluctuations in black lipid-membranes. Biophys. J. 38, 251–258.

Hladky, S.B., Gruen, D.W.R., 1984. Energetics of fluctuation in lipid Bilayer thickness—response. Biophys. J. 45, 645–646.

Holthuis, J.C.M., van Meer, G., Huitema, K., 2003. Lipid microdomains, lipid translocation and the organization of intracellular membrane transport (Review). Mol. Membrane Biol. 20, 231–241.

Huang, H.W., 1986. Deformation free-energy of Bilayer-membrane and its effect on gramicidin channel lifetime. Biophys. J. 50, 1061–1070.

Karatekin, E., Sandre, O., Guitouni, H., Borghi, N., Puech, P.H., Brochard-Wyart, F., 2003. Cascades of transient pores in giant vesicles: Line tension and transport. Biophys. J. 84, 1734–1749.
Kessel, A., Ben Tal, N., May, S., 2001. Interactions of cholesterol with lipid bilayers: The preferred configuration and fluctuations. Biophys. J. 81, 643–658.
Leontiadou, H., Mark, A.E., Marrink, S.J., 2004. Molecular dynamics simulations of hydrophilic pores in lipid bilayers. Biophys. J. 86, 2156–2164.
Litster, J.D., 1975. Stability of lipid Bilayers and red blood-cell membranes. Phys. Lett. A 53, 193–194.
Loison, C., Mareschal, M., Schmid, F., 2004. Pores in bilayer membranes of amphiphilic molecules: Coarse-grained molecular dynamics simulations compared with simple mesoscopic models. J. Chem. Phys. 121, 1890–1900.
Marrink, S.J., Lindahl, E., Edholm, O., Mark, A.E., 2001. Simulation of the spontaneous aggregation of phospholipids into bilayers. J. Am. Chem. Soc. 123, 8638–8639.
May, S., 2000. Protein-induced bilayer deformations: The lipid tilt degree of freedom. Eur. Biophys. J. Biophys. Lett. 29, 17–28.
Moroz, J.D., Nelson, P., 1997. Dynamically stabilized pores in bilayer membranes. Biophys. J. 72, 2211–2216.
Movileanu, L., Popescu, D., 1995. Differential length effects in a binary mixture of single-chain amphiphiles in planar monolayers: A 3-dimensional approach. Biosystems 36, 43–53.
Movileanu, L., Popescu, D., 1996. Global ratio of efficiency in a single chain binary mixture. J. Biol. Systems 4, 425–432.
Movileanu, L., Popescu, D., Victor, G., Turcu, G., 1997. Selective association of phospholipids as a clue for the passive flip-flop diffusion through bilayer lipid membranes. Biosystems 40, 263–275.
Movileanu, L., Popescu, D., 1998. A theoretical model for the association probabilities of saturated phospholipids from two-component bilayer lipid membranes. Acta Biotheor. 46, 347–368.
Movileanu, L., Popescu, D., Flonta, M.L., 1998. The hydrophobic acyl-chain effect in the lipid domains appearance through phospholipid bilayers. Theochem. J. Mol. Struct. 434, 213–227.
Movileanu, L., Popescu, D., 2004. The birth, life and death of statistical pores into a bilayer membrane. In: Recent Research Developments in Biophysics. Transworld Research Network, Kerala, pp. 61–86.
Neher, E., Eibl, H., 1977. Influence of Phospholipid Polar Groups on Gramicidin Channels. *Biochim. Biophys. Acta* 464, 37-44.
Neu, J.C., Krassowska, W., 2003. Modeling postshock evolution of large electropores. Phys. Rev. E 67, 2191–2195
Neu, J.C., Smith, K.C., Krassowska, W., 2003. Electrical energy required to form large conducting pores. Bioelectrochemistry 60, 107–114.
Nielsen, C., Goulian, M., Andersen, O.S., 1998. Energetics of inclusion-induced bilayer deformations. Biophys. J. 74, 1966–1983.
Nielsen, C., Andersen, O.S., 2000. Inclusion-induced bilayer deformations: Effects of monolayer equilibrium curvature. Biophys. J. 79, 2583–2604
Partenskii, M.B., Dorman, V.L., Jordan, P.C., 1998. Membrane stability under electrical stress: A nonlocal electroelastic treatment. J. Chem. Phys. 109, 10361–10371.
Pastushenco, V.F., Chizmadzev Yu, A., Arakelyan, V.B., 1979. Electric breakdown of Bilayer lipid membranes. II. Calculation of the membrane lifetime in the steady state diffusion approximation. Bioelectrochem. Bioenergetics 6, 53–62.
Popescu, D., Margineanu, D.G., 1981. Intramembrane interactions and breakdown of lipid bilayers. Bioelectrochem. Bioenerg. 8, 581–583.
Popescu, D., Victor, G., 1990. Association probabilities between the single chain amphiphiles into a binary mixture in planar monolayers. Biochim. Biophys. Acta 1030, 238–250.
Popescu, D., Rucareanu, C., Victor, G., 1991. A Model for the appearance of statistical pores in membranes due to selfoscillations. Bioelectrochem. Bioenerg. 25, 91–103.
Popescu, D., Victor, G., 1991a. Calculation of the optimal surface-area for amphiphile molecules using the hard-core method. Biophys. Chem. 39, 283–286.
Popescu, D., Victor, G., 1991b. The transversal diffusion-coefficient of phospholipid molecules through black lipid-membranes. Bioelectrochem. Bioenerg. 25, 105–108.

Popescu, D., Rucareanu, C., 1992. Membrane selfoscillations model for the transbilayer statistical pores and flip-flop diffision. Mol. Cryst. Liquid Cryst. 25, 339–348.
Popescu, D., 1993. Association probabilities between the single-chain amphiphiles into a binary mixture in plan monolayers (II). Biochim. Biophys. Acta 1152, 35–43.
Popescu, D., Movileanu, L., Victor, G., Turcu, G., 1997. Stability and instability properties of aggregation of single chain amphiphiles into binary mixtures. Bull. Math. Biol. 59, 43–61.
Popescu, D., Ion, S., Popescu, A.I., Movileanu, L., 2003. Elastic properties of bilayer lipid membranes and pore formation. In: Ti Tien, H., Ottova, A. (Eds.), Planar Lipid Bilayers (BLMs) and Their Applications. Elsevier Science Publishers, Amsterdam, pp. 173–204.
Rawicz, W., Olbrich, K.C., McIntosh, T., Needham, D., Evans, E., 2000. Effect of chain length and unsaturation on elasticity of lipid bilayers. Biophys. J. 79, 328–339.
Sackmann, E., 1995. Biological membranes: architecture and function. In: Lipowsky, R., Sackmann, E. (Eds.), Structure and Dynamics of Membranes. Elsevier/North-Holland, Amsterdam, pp. 1–63.
Saulis, G., 1997. Pore disappearance in a cell after electroporation: Theoretical simulation and comparison with experiments. Biophys. J. 73, 1299–1309.
Schneider, M.B., Jenkins, J.T., Webb, W.W., 1984. Thermal fluctuations of large quasi-spherical bimolecular phospholipid-vesicles. J. Physique 45, 1457–1472.
Shillcock, J.C., Boal, D.H., 1996. Entropy-driven instability and rupture of fluid membranes. Biophys. J. 71, 317–326.
Shillcock, J.C., Seifert, U., 1998. Thermally induced proliferation of pores in a model fluid membrane. Biophys. J. 74, 1754–1766.
Sung, W., Park, P.J., 1997. Dynamics of pore growth in membranes and membrane stability. Biophys. J. 73, 1797–1804.
Sung, W.Y., Park, P.J., 1998. Transition dynamics of biological systems on mesoscopic scales: Effects of flexibility and fluctuations. Physica A 254, 62–72.
Tieleman, D.P., Leontiadou, H., Mark, A.E., Marrink, S.J., 2003. Simulation of pore formation in lipid bilayers by mechanical stress and electric fields. J. Am. Chem. Soc. 125, 6382–6383.
Tieleman, D.P., 2004. The molecular basis of electroporation. BMC Biochem. 5, 1–12.
White, S.H., 1978. Formation of solvent-free black lipid bilayer membranes from glyceryl monooleate dispersed in squalene. Biophys. J. 23, 337–347.
Winterhalter, M., Helfrich, W., 1987. Effect of voltage on pores in membranes. Phys. Rev. A 36, 5874–5876.
Zhelev, D.V., Needham, D., 1993. Tension-stabilized pores in giant vesicles: Determination of pore-size and pore line tension. Biochim. Biophys. Acta 1147, 89–104.